





RESEARCH ARTICLE | APRIL 04 2025

A capacitance-coupled Ga_2O_3 memristor

Alfred Moore ; Lijie Li ; Hang Shao; Xiaoyan Tang; Huili Liang; Zengxia Mei; Yaonan Hou  *AIP Advances* 15, 045309 (2025)<https://doi.org/10.1063/5.0260023>

Articles You May Be Interested In

Investigation of resistive switching and transport mechanisms of $\text{Al}_2\text{O}_3/\text{TiO}_{2-x}$ memristors under cryogenic conditions (1.5 K)

AIP Advances (February 2020)

Voltage-programmable negative differential resistance in memristor of single-crystalline lithium niobate thin film

Appl. Phys. Lett. (January 2022)

Memristor and selector devices fabricated from $\text{HfO}_{2-x}\text{N}_x$

Appl. Phys. Lett. (April 2016)



Special Topics Open for Submissions

[Learn More](#)

A capacitance-coupled Ga₂O₃ memristor

Cite as: AIP Advances 15, 045309 (2025); doi: 10.1063/5.0260023

Submitted: 4 February 2025 • Accepted: 22 March 2025 •

Published Online: 4 April 2025



Alfred Moore,¹ Lijie Li,^{1,2,a)} Hang Shao,³ Xiaoyan Tang,³ Huili Liang,^{3,4} Zengxia Mei,^{3,4,b)} and Yaonan Hou^{1,2,c)}

AFFILIATIONS

¹ Electronic and Electrical Engineering, Swansea University, Bay Campus, SA1 8EN Swansea, United Kingdom

² Centre for Integrative Semiconductor Materials (CISM), Swansea University, Bay Campus, SA1 8EN Swansea, United Kingdom

³ Songshan Lake Materials Laboratory, Dongguan, Guangdong 523808, China

⁴ Institute of Physics, Chinese Academy of Sciences, Beijing 100190, China

a) l.li@swansea.ac.uk

b) zxmei@iphy.ac.cn

c) Author to whom correspondence should be addressed: yaonan.hou@swansea.ac.uk

ABSTRACT

Memristors are regarded as a key electronic component for non-von Neumann computing, such as neuromorphic networks. Hereby, we report a capacitance-coupled memristor (C-memristor) configured with ITO/Ga₂O₃/ITO coplanar interdigital structures. Depending on the voltage sweeping directions, the C-memristor exhibits a clear current switching with different polarities, offering an easy-to-readout electronic status. Due to the coupled capacitance, the difference between the currents in forward and reverse scanning strongly depends on the voltage sweeping speed, which was quantitatively studied with an equivalent circuit that we established. A device model based on filamentary conductive paths formed by the electrically driven oxygen vacancies was utilized to explain the working mechanism of the C-memristor, which aligns well with the observed results. Unlike previously reported Ga₂O₃ memristors that rely only on the status of the resistance, our device also exhibits capacitance variation, offering an additional degree of freedom (e.g., the power nodes) for constructing a neural network.

© 2025 Author(s). All article content, except where otherwise noted, is licensed under a Creative Commons Attribution (CC BY) license (<https://creativecommons.org/licenses/by/4.0/>). <https://doi.org/10.1063/5.0260023>

I. INTRODUCTION

A memristor is a nonlinear resistance switching device, regarded as a promising electronic component for neuromorphic computing as a scheme for realizing artificial intelligence (AI).¹ The device was predicted by Leon Chua as the fourth fundamental electronic component in addition to resistor, capacitor, and inductor in 1971, when he investigated the relationship between each two out of the four circuit variables, namely, current i , voltage v , charge q , and magnetic flux ϕ .² The first solid-state memristor was realized by Strukov *et al.* from HP labs in 2008.³ Subsequently, memristors have been developing rapidly, including single devices with various working mechanisms and neuro-network systems.^{4–8} The typical feature of a memristor is that the device remembers its previous resistance based on the history of the voltage applied,⁹ reflected by a hysteresis loop in the current–voltage (IV) characteristics.

Many materials have been developed to fabricate memristors, including binary oxides, perovskites, and two-dimensional materials.¹⁰ Among them, binary oxides (e.g., TiO_x, ZrO_x, and ZnO_x) are the largest material group due to their easy fabrication and strong current hysteresis.^{11–13} Ga₂O₃ as a new binary oxide semiconductor material (fourth-gen semiconductor) demonstrates its great potential in various fields, including power electronics, radiation detectors, and memristors.^{14–18} So far, nearly all published studies on Ga₂O₃ memristors focus on the changing of resistivity, while the effects of capacitance have yet to be understood.

In this work, we fabricated an ITO/Ga₂O₃/ITO coplanar interdigital device, which exhibits current hysteresis assisted with a coupled variable capacitance. By using an equivalent circuit, the behavior of the device can be quantitatively analyzed. Based on this, the device working mechanism can be well explained with a conductive filament model.

II. EXPERIMENTS

A 150 nm undoped Ga_2O_3 film was deposited on a quartz substrate by radio frequency sputtering with a Ga_2O_3 target under a power of 60 W. The sputtering pressure was 0.4 Pa, and the substrate was not intentionally heated. Details of growth can be found elsewhere.^{19–21} The surface of the film shows a mirror-like flatness, with a measured roughness <1 nm in a $3 \times 3 \mu\text{m}^2$ scan area by atomic force microscopy (Fig. S1 of the [supplementary material](#)). As indicated by x-ray diffraction measurement (Fig. S2 of the [supplementary material](#)), the material is amphoteric Ga_2O_3 (a- Ga_2O_3).^{19,22} The transmittance/reflectance measurements show that the bandgap of the material is around 4.8 eV (Fig. S3 of the [supplementary material](#)).²² X-ray photoelectron spectroscopy (XPS) shows oxygen binding energy at 530.8 and 531.7 eV [Fig. 1(a)], corresponding to the lattice oxygen of Ga_2O_3 and oxygen vacancy (VO) related defects. It should be noted that the peak at 531.7 eV indicates the existence of oxygen vacancies.²² The device was fabricated by depositing ITO interdigital electrodes on the film with standard UV lithography. The gap between two ITO interdigital electrodes is $5 \mu\text{m}$, with 75 pairs in total [Fig. 1(b)]. The electronic property of the device was measured using a probe station in an electronically shielded box equipped with a Keithley 2636B source meter (SMU), with a current resolution down to 2 fA. The alternative current (AC) frequency response was measured with a function generator (Rohde and Schwarz HMF2525) and a digital oscilloscope (Rohde and Schwarz RTB2002).

III. RESULTS AND DISCUSSION

Figure 1(c) displays a loop-IV curve measured from -20 to 20 V. A prominent current hysteresis can be observed. When the voltage is sweeping from negative (positive) to positive (negative), the current increases with a resistance switching behavior (negative resistance) appearing at around $+7$ (-7) V, a typical memristor characteristic. We focus on the voltage ranging from -9 to 9 V [highlighted region in Fig. 1(c)], as the difference in current values between the half loops is more pronounced in this region. Figure 1(d) shows the closed view of this region, where the IV curve is symmetry in terms of the first (red) and second (blue) half loops. One important feature is that the current increases (decreases) with increasing (decreasing) sweeping voltage, along with a positive (negative) current generated even when the voltage is negative (positive), while the IV curve does not pass through the origin. Therefore, it is reasonable to conclude the presence of a capacitance. It is worth mentioning that the power consumption of our device is estimated below 10 nW in the working voltage range from -9 to 9 V [Fig. 1(d)], which potentially leverages the energy-efficient memristor-based neural networks. Figure 1(e) plots the current at 6 V measured in 100 loops. It is found that the current ratio in forward (I_F) and reverse (I_R) is $+1/-0.7$ nA with no degradation, indicating good repeatability. The improvement of the current in the first 40 loops could be due to the improvement of the oxygen vacancy gradient related to the bias history, as suggested by Aoki *et al.*²³ The current polarity offers easy-to-readout electronic

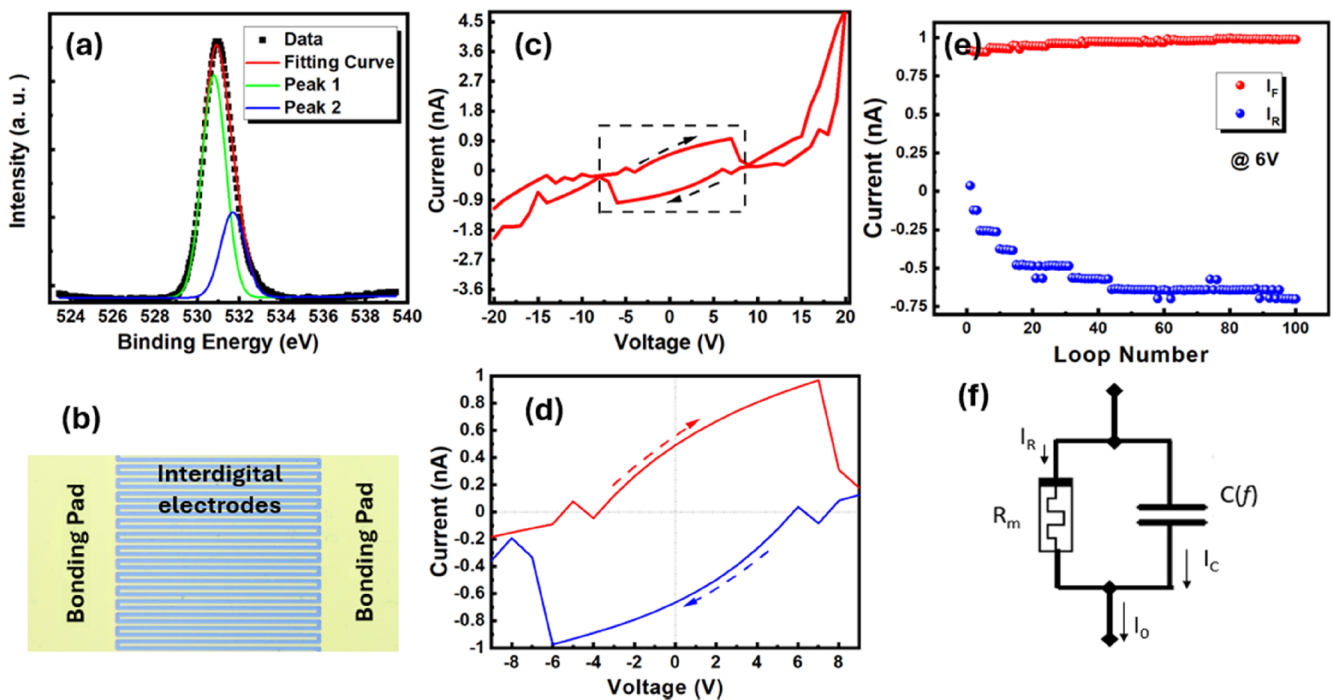


FIG. 1. (a) XPS spectrum of the oxygen peaks, (b) zoom-in of the interdigital electrodes (a full image can be found in Fig. S4 of the [supplementary material](#)), (c) full-range IV curve from -20 to 20 V, (d) zoom-in IV curve in the highlighted region in (c), (e) current at 6 V in 100 loop measurements, and (f) the proposed equivalent circuit.

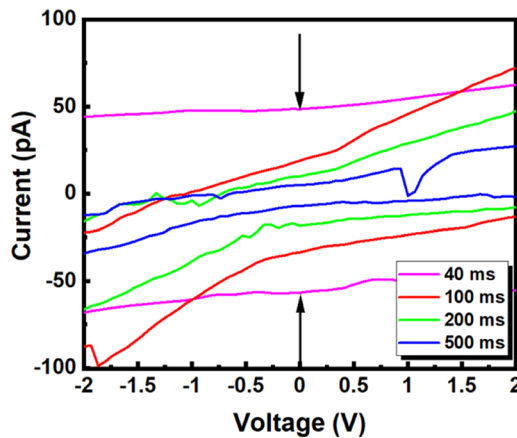


FIG. 2. IV curves near $V = 0$ with various sweeping times (time between each step) from 40 to 500 ms.

states of a memristor, which differs from previous Ga_2O_3 memristors that rely only on resistance values. In order to explain the device working mechanism, we proposed an equivalent circuit as shown in Fig. 1(f), where a variable capacitor $[C(f)]$ is coupled to the memristor (R_m). The total current (I_0) of the device is the sum of the current through the memristor I_R and the one through the capacitor I_C ,

$$\begin{aligned} I_0 &= I_R + I_C \\ &= \frac{V}{R_m} + C(f) \frac{dV}{dt} \\ &= \frac{V}{R_m} + C(f) \frac{\Delta V}{\Delta t}, \end{aligned} \quad (1)$$

where $\frac{\Delta V}{\Delta t}$ is the voltage sweeping speed in IV measurement. From Eq. (1), the polarity of the total current is determined not only by V but also by the sweeping rate and directions. This explains the negative (positive) current at a positive (negative) voltage in Fig. 1(d). In the measurements of Figs. 1(c) and 1(d), the sweeping speed is ~ 66.7 mV/20 ms and then a capacitance of 27 pF is obtained. It is

worth mentioning that the capacitance could be variable when the electronic status changes in the device, as was proved later in this work.

When $V = 0$, the current is solely dependent on capacitance and the sweeping speed, which will be reflected by the difference between I_F and I_R (defined as “opening” in this paper). To prove this prediction, IV measurements with various sweep speeds have been carried out. The near $V = 0$ IV plots are shown in Fig. 2. Obviously, the opening decreases with decreasing sweeping speed (or increasing step time in the measurement), indicating that the total value of $C(f) \frac{\Delta V}{\Delta t}$ is decreasing. At the same time, an oscillation of current with the applied voltage can be observed, with variable peak-to-peak amplitude and period related to the voltage sweeping speed (Fig. S5 of the supplementary material).

In order to understand the working mechanism, we further analyzed the capacitance at different sweeping speeds. Figure 3 shows the capacitance obtained at $V = 0$ from Eq. (1), plotted as a function of $\frac{\Delta V}{\Delta t}$. The result indicates that the capacitance is not a constant, with a decreasing value with increasing sweeping speed. A conducting filament model schematically shown in Fig. 3(b) is used to understand our device.^{24–27} When there is no bias, the oxygen vacancies are distributed randomly inside Ga_2O_3 , where no conductive filament forms. Under an external bias, the oxygen vacancies are driven toward the direction of the electrode, and adjacent vacancies subsequently form a conductive filament. Different from the existing reports where a very thin Ga_2O_3 film (<100 nm) was employed to facilitate the filament connecting two electrodes,^{28–30} the distance between two electrodes is $5 \mu\text{m}$ in our device. Therefore, the conductive filaments do not span the entire device. Instead, only the length of the non-filament region (d) is reduced. As a result, the resistance ($R \propto l - d$, where l is the length of the material between two electrodes) will decrease and capacitance will increase ($C \propto \frac{1}{d}$). Regarding the current oscillation, it is attributed to temporal polarization and depolarization processes [Fig. 3(c)].³¹

Finally, we measured the AC response of our C-memristor. The top panel (black curve) of Fig. 4(a) shows an applied square wave at 7 kHz, while the bottom one (red curve) shows the measured response of the C-memristor. By fitting the time decay into $I = A \exp\left(-\frac{t}{\tau}\right) + B$ (where A, B, τ are fitting parameters), a time

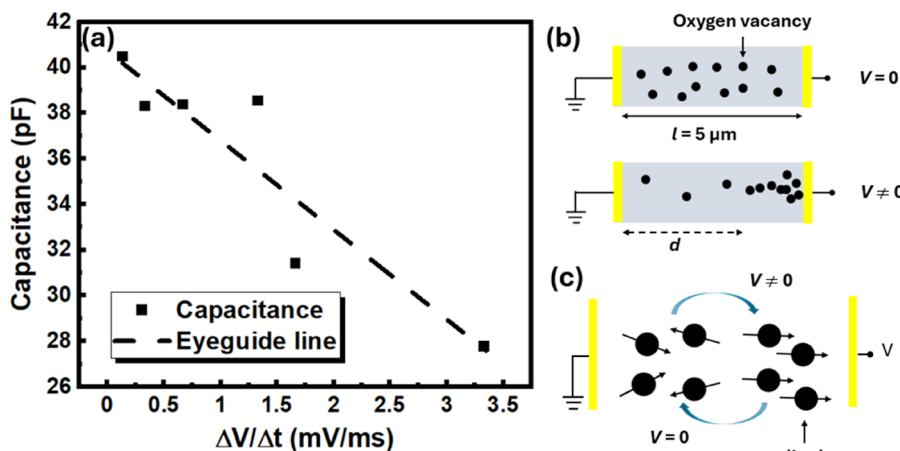


FIG. 3. (a) Capacitance as a function of sweeping speed, (b) schematic of the conductive filament model, and (c) schematic of polarization and depolarization processes.

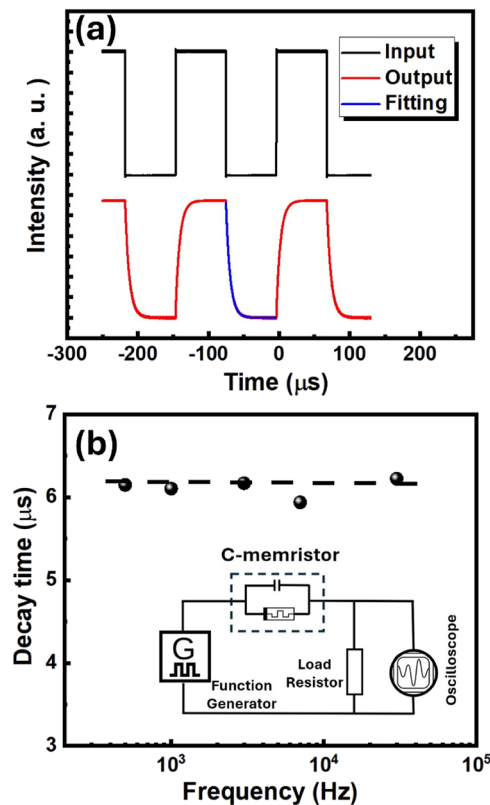


FIG. 4. (a) AC response of the C-memristor and (b) extracted time decay measured at different frequencies up to 30 kHz (the inset shows the schematic of the setup).

decay of $\tau = 5.9 \mu\text{s}$ was obtained (blue curve), corresponding to a maximum working frequency of $\sim 169 \text{ kHz}$. Figure 4(b) shows the measurements up to 30 kHz with our current setup, exhibiting a stable time constant.

IV. CONCLUSION

In summary, we have realized a C-memristor based on a Ga_2O_3 film with ITO interdigital electrodes. The device exhibits a clear current hysteresis with coupled capacitance, where the latter decides the current differences between forward and reverse scanning (speed). We established an equivalent circuit for quantitatively studying the details of electrical properties. Together with a conductive filament model, the results and device working mechanism can be well explained. In addition, the device offers facilitated readout binary electronic states (polarity) and a fast-working frequency of up to 169 kHz. We envisage that coupled capacitance will offer an additional degree of freedom for building memristor-based neural networks.^{1,32,33}

SUPPLEMENTARY MATERIAL

See the [supplementary material](#) for the surface flatness measured by AFM (Fig. S1), XRD scans (Fig. S2), transmittance/reflectance measurements (Fig. S3), a full-image of the device

(Fig. S4), and detailed IV measurements at various voltage sweeping speeds (Fig. S5).

ACKNOWLEDGMENTS

This work was supported by the EPSRC under Grant No. EP/T019085/1, Royal Society under Grant No. IEC\NSFC\242145, and SACEME Seedcorn funding from Swansea University. H.L. and Z.M. thank the National Natural Science Foundation of China for the support under Grant Nos. 12174275 and 62174113.

AUTHOR DECLARATIONS

Conflict of Interest

The authors have no conflicts to disclose.

Author Contributions

Alfred Moore: Formal analysis (equal); Investigation (equal); Methodology (equal); Writing – original draft (equal); Writing – review & editing (equal). **Lijie Li:** Conceptualization (equal); Formal analysis (equal); Investigation (equal); Methodology (equal); Resources (equal); Supervision (lead); Writing – original draft (equal); Writing – review & editing (equal). **Hang Shao:** Methodology (equal). **Xiaoyan Tang:** Methodology (equal). **Huili Liang:** Funding acquisition (equal); Methodology (equal); Resources (equal); Supervision (equal); Writing – original draft (equal); Writing – review & editing (equal). **Zengxia Mei:** Funding acquisition (equal); Methodology (equal); Resources (equal); Supervision (equal); Writing – original draft (equal); Writing – review & editing (equal). **Yaonan Hou:** Conceptualization (lead); Data curation (equal); Formal analysis (lead); Funding acquisition (equal); Methodology (equal); Project administration (lead); Resources (equal); Supervision (equal); Writing – original draft (lead); Writing – review & editing (lead).

DATA AVAILABILITY

The data that support the findings of this study are available from the corresponding author upon reasonable request.

REFERENCES

- F. Aguirre, A. Sebastian, M. Le Gallo, W. Song, T. Wang, J. J. Yang, W. Lu, M.-F. Chang, D. Ielmini, Y. Yang, A. Mehonic, A. Kenyon, M. A. Villena, J. B. Roldán, Y. Wu, H.-H. Hsu, N. Raghavan, J. Suñé, E. Miranda, A. Eltawil, G. Setti, K. Smagulova, K. N. Salama, O. Krestinskaya, X. Yan, K.-W. Ang, S. Jain, S. Li, O. Alharbi, S. Pazos, and M. Lanza, *Nat. Commun.* **15**(1), 1974 (2024).
- L. Chua, *IEEE Trans. Circuit Theory* **18**(5), 507–519 (1971).
- D. B. Strukov, G. S. Snider, D. R. Stewart, and R. S. Williams, *Nature* **443**(7191), 80–83 (2008).
- M. Gabel and Y. Gu, *Adv. Funct. Mater.* **31**(9), 2009999 (2021).
- J. H. Yoon, Z. Wang, K. M. Kim, H. Wu, V. Ravichandran, Q. Xia, C. S. Hwang, and J. J. Yang, *Nat. Commun.* **9**(1), 417 (2018).
- T. Fu, X. Liu, H. Gao, J. E. Ward, X. Liu, B. Yin, Z. Wang, Y. Zhuo, D. J. F. Walker, J. Joshua Yang *et al.*, *Nat. Commun.* **11**(1), 1861 (2020).
- T. Emmerich, Y. Teng, N. Ronceray, E. Lopriore, R. Chiesa, A. Chernev, V. Artemov, M. Di Ventra, A. Kis, and A. Radenovic, *Nat. Electron.* **7**(4), 271–278 (2024).
- X. Zhu, Q. Wang, and W. D. Lu, *Nat. Commun.* **11**(1), 2439 (2020).

- ⁹B. Tellini, M. Bologna, K. J. Chandía, and M. Macucci, *Int. J. Circuit Theory Appl.* **49**(11), 3488–3506 (2021).
- ¹⁰A. R. Patil, T. D. Dongale, R. K. Kamat, and K. Y. Rajpure, *Mater. Today Commun.* **34**, 105356 (2023).
- ¹¹F. Profumo, F. Borghi, A. Falqui, and P. Milani, *J. Phys. D: Appl. Phys.* **56**(35), 355301 (2023).
- ¹²Y. She, F. Wang, X. Zhao, Z. Zhang, C. Li, H. Pan, K. Hu, Z. Song, and K. Zhang, *IEEE Trans. Electron Devices* **68**(4), 1950–1955 (2021).
- ¹³F. M. Simanjuntak, T. Ohno, and S. Samukawa, *ACS Appl. Electron. Mater.* **1**(11), 2184–2189 (2019).
- ¹⁴M. Higashiwaki, *AAPPS Bull.* **32**(1), 3 (2022).
- ¹⁵A. J. Green, J. Speck, G. Xing, P. Moens, F. Allerstam, K. Gumaelius, T. Neyer, A. Arias-Purdue, V. Mehrotra, A. Kuramata *et al.*, *APL Mater.* **10**(2), 029201 (2022).
- ¹⁶B. R. Tak, S. Kumar, A. K. Kapoor, D. Wang, X. Li, H. Sun, and R. Singh, *J. Phys. D: Appl. Phys.* **54**(45), 453002 (2021).
- ¹⁷D. Kaur and M. Kumar, *Adv. Opt. Mater.* **9**(9), 2002160 (2021).
- ¹⁸X. Chen, F.-F. Ren, J. Ye, and S. Gu, *Semicond. Sci. Technol.* **35**(2), 023001 (2020).
- ¹⁹R. Zhu, H. Liang, S. Liu, Y. Yuan, X. Wang, F. C.-C. Ling, A. Kuznetsov, G. Zhang, and Z. Mei, *Nat. Commun.* **14**(1), 5396 (2023).
- ²⁰R. Zhu, H. Liang, S. Hu, Y. Wang, and Z. Mei, *Adv. Electron. Mater.* **8**(1), 2100741 (2022).
- ²¹H. Liang, S. Cui, R. Su, P. Guan, Y. He, L. Yang, L. Chen, Y. Zhang, Z. Mei, and X. Du, *ACS Photonics* **6**(2), 351–359 (2019).
- ²²H. Liang, X. Tang, H. Shao, R. Zhu, S. Deng, X. Zhan, T. Zhu, J. Wang, J. Zhang, G. Zhang, and Z. Mei, *Adv. Sci.* **11**(48), 2410761 (2024).
- ²³Y. Aoki, C. Wiemann, V. Feyer, H.-S. Kim, C. M. Schneider, H. Ill-Yoo, and M. Martin, *Nat. Commun.* **5**(1), 3473 (2014).
- ²⁴M. Sparvoli, J. F. D. Chubaci, F. O. Jorge, D. G. Fidelis, G. S. Goveia, T. F. Silva, C. L. Rodrigues, A. Ferreira, R. D. Mansano, and J. A. Freitas, *Phys. Status Solidi B* (published online).
- ²⁵L.-W. Wang, C.-W. Huang, K.-J. Lee, S.-Y. Chu, and Y.-H. Wang, *Nanomaterials* **13**(12), 1851 (2023).
- ²⁶X. Dai, X. Zhang, D. Gong, and G. Xiang, *Adv. Funct. Mater.* **33**(49), 2304749 (2023).
- ²⁷M. W. Alam, A. Jamir, B. Longkumer, B. Souayah, S. Sadaf, and B. Moirangthem, *J. Alloys Compd.* **1010**, 177032 (2025).
- ²⁸N. Masaoka, Y. Hayashi, T. Tohei, and A. Sakai, *Jpn. J. Appl. Phys.* **62**, SC1035 (2023).
- ²⁹H. J. Lee, J.-H. Kim, J. Choi, Y. S. Kim, and S.-N. Lee, *Heliyon* **9**(12), e23157 (2023).
- ³⁰H. J. Lee, J.-H. Kim, H.-J. Kim, and S.-N. Lee, *Materials* **17**(11), 2727 (2024).
- ³¹H. Morkoç, R. Cingolani, and B. Gil, *Mater. Res. Innovations* **3**, 97–106 (1999).
- ³²J. Yang, R. Mao, M. Jiang, Y. Cheng, P.-S. V. Sun, S. Dong, G. Pedretti, X. Sheng, J. Ignowski, H. Li, C. Li, and A. Basu, *Nat. Commun.* **16**(1), 1136 (2025).
- ³³B. Gao, Y. Zhou, Q. Zhang, S. Zhang, P. Yao, Y. Xi, Q. Liu, M. Zhao, W. Zhang, Z. Liu, X. Li, J. Tang, H. Qian, and H. Wu, *Nat. Commun.* **13**(1), 2026 (2022).